MDPI

*Article*

# Marangoni Bursting: Insight into the Role of the Thermocapillary Effect in an Oil Bath

Michalina Ślemp [1,2] and Andrzej Miniewicz [1,*]

1   Institute of Advanced Materials, Faculty of Chemistry, Wroclaw University of Science and Technology, 50-370 Wroclaw, Poland; michalina.slemp@gmail.com
2   Non-Linear Optical and Interfaces Group, Institute of Light and Matter, Claude Bernard University Lyon 1, 69622 Villeurbane, France
*   Correspondence: andrzej.miniewicz@pwr.edu.pl

**Abstract:** Marangoni bursting describes the spontaneous spread of a droplet of a binary mixture of alcohol/water deposited on a bath of oil, followed by its fast spontaneous fragmentation into a large number of smaller droplets in a self-similar way. Several papers have aimed to describe the physical phenomena underlying this spectacular phenomenon, in which two opposite effects, solutal and thermal Marangoni stresses, play competitive roles. We performed investigations of the Marangoni bursting phenomenon, paying attention to the surface temperature changes during bursting and after it. Fragmentation instabilities were monitored using a thermal camera for various initial alcohol/water compositions and at different stages of the process. We uncovered the role of thermocapillary Marangoni flows within the more viscous oil phase that are responsible for outward and inward shrinking of the periphery circle at the final stage of the phenomenon, enabling a more comprehensive understanding of the thermal Marangoni effect. Simulations of the Marangoni thermocapillary effect in an oil bath by solving coupled Navier–Stokes and heat transport equations using the COMSOL Multiphysics software platform support our experimental observations.

**Keywords:** Marangoni solutal and thermocapillary effect; Marangoni bursting; spreading fingering instability; binary mixture droplet evaporation; infrared thermography

## 1. Introduction

Marangoni solutal and thermocapillary effects have been known for more than one hundred years from the pioneering works of Carlo Marangoni [1–3]. As detailed in these works, the physical grounds of the famous 'tears of wine' as a result of a delicate balance between bulk and interfacial hydrodynamics were recently revisited in work by Venerus and Simavilla [4], who pointed out the importance of temperature gradients and not the concentration gradients alone. Generally, the Marangoni stresses arising due to concentration or temperature gradients produce respective surface tension ($\gamma$) gradients, $\overrightarrow{\nabla}_s \gamma$, that generate near surface liquid flows. These flows are useful and/or cannot be neglected in many technological processes where liquid phases are involved, including in metallurgy [5–7], the semiconductor industry [8–10], medicine [11,12], biology [13], opto- and microfluidics [14–16] and nanotechnology [17,18]. Together with investigations of new multiphase liquid systems in biology and interactions between liquids and nanoparticles, micro-objects and gas bubbles [19] in the presence of structured light, a deep understanding of all aspects of the Marangoni phenomenon is of utmost importance. In particular, all effects related to the spreading of a drop of binary liquid on a liquid substrate have attracted the interest of several groups studying the interfaces between two or more fluids. Depending on the system studied, the temperature and concentration or surfactant concentration produce ubiquitous liquid–liquid Marangoni stresses. There are reports on interfacial bursting [20], film spreading [21–23], fingering instability [24,25], de-wetting [26,27] and even liquid jet

instabilities with ligament break-up [28]. The interplay of these effects may result in the appearance of dynamic organized patterns [29,30].

The excellent example of an unusual Marangoni bursting phenomenon occurring in a three-phase alcohol/water/oil system was first described and studied by Keiser et al. [30]. It is a piece of nontrivial physics originating from both solutal and thermocapillary Marangoni effects interplaying at the same time. Spectacular spontaneously occurring fragmentation of isopropyl alcohol/water droplet of a certain specific composition deposited over an oil bath has attracted the attention of a broad audience due to the regularity and beauty of this process, captured in movies and published in the Supplementary Materials of the original publication by Keiser et al. [30,31]. Marangoni bursting, occurring due to spreading and retraction of evaporating droplet comprising volatile binary mixtures over solid or liquid surfaces, initiated several attempts to study its various aspects [32–43] and related phenomena (see the extensive list of references in the work by Williams [41]). Recently, Hasegawa and Manzaki [43] studied the thermal Marangoni effect during the bursting process and visualized the temperature field with a thermal camera, concluding that Marangoni convection influences the spreading behavior. Seyfert and Marin [44] addressed the influence of dye added to initial binary solution on droplet instability and concluded that the amount of dye can significantly change the droplet size distribution and fingering instability conditions.

In this work, we would like to investigate the Marangoni bursting process by analyzing the dynamics of droplet spreading via measurements of the thermal radiation field from the whole oil pool using a precise thermal FLIR E96 camera. In particular, we focused our attention on the evolution of the binary droplets after the atomization process, trying to find out the physical reason for the slow shrinking of the outer ring of radius R (Figures 1 and 2 and Electronic Supplementary Information, ESI Videos S2, S3 and S5), because this process was not addressed in detail in previous studies of the Marangoni bursting phenomenon.
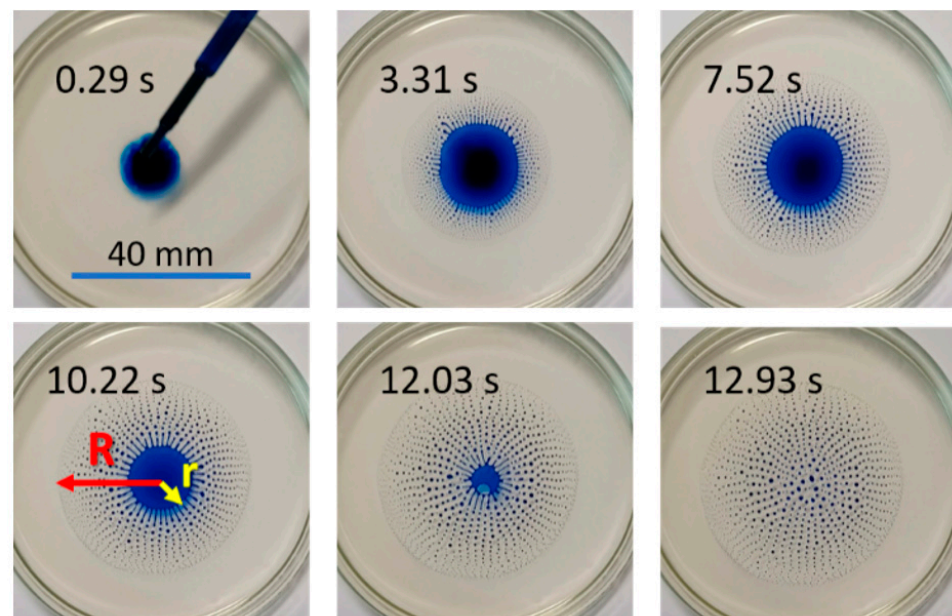


**Figure 1.** Sequence of photographs presenting the behavior of a drop of the binary mixture containing isopropanol and water ($\phi_0 = 0.45$) deposited on the surface of pure rapeseed oil. In this preliminary experiment, brilliant blue dye was added to the solution to improve the visibility of the Marangoni bursting phenomenon. Each photograph is labelled with time elapsed from $t = 0$ s when the drop came into contact with the oil surface. The red arrow shows the radius of the outer ring $R$, marking the position of the daughter droplet manifold, and the yellow arrow shows the radius $r$ of the mother drop edge.
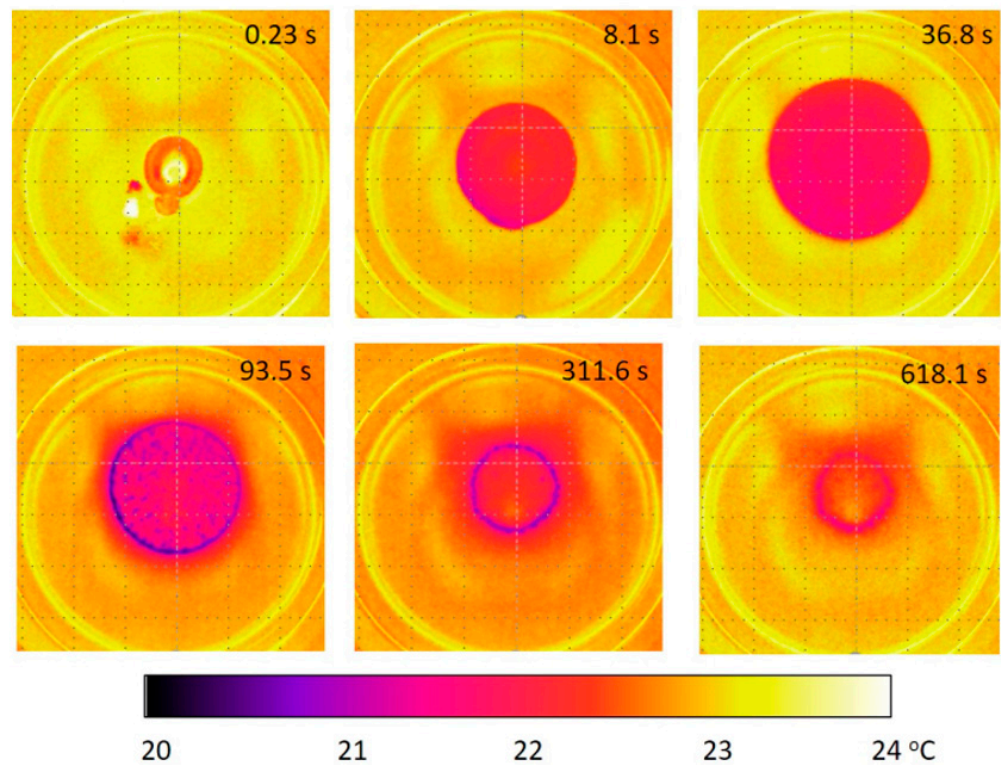
**Figure 2.** Dynamics of Marangoni busting process observed by a calibrated thermal camera for the IPA/water binary mixture with ($\phi_0$ = 0.45) deposited over pure rapeseed oil layer. No dye is added to the initial binary mixture. The observation period extends up to ~10 min. The color temperature scale is given at the bottom. The inner diameter of a Petri dish is 70 mm.

## 2. Materials and Methods

### 2.1. Materials

Isopropyl alcohol, IPA, $C_3H_8O$ (POCH, Gliwice, Poland) was mixed with distilled water in 2:5 to 4:5 w/w proportions (the initial mass fraction $\phi_0$ = 0.4 to 0.8 after [31]). A methyl blue acid dye ($C_{37}H_{27}N_3Na_2O_9S_3$, Sigma Aldrich, St. Louis, MO, USA), perfectly soluble in water, was added to the mixture for clear visualization of the fingering instability in visible light. The concentration of dye $c_{MB}$ [mg·(mL)$^{-1}$] was calculated from the mass of methyl blue dissolved per volume of the binary mixture IPA/water. We also use the brilliant blue dye E133 ($C_{37}H_{34}N_2Na_2O_9S_3$, Sigma Aldrich, St. Louis, MO, USA) for coloring purposes. The physicochemical properties of the key substances used in the present study are listed in ESI (Figure S3, Tables S1 and S2).

### 2.2. Methods

We prepared a rapeseed oil pool in a Petri dish with an inner diameter of 70 mm. The oil pool depth amounted to $H \approx 5$ mm. Then, the binary solution was drawn up with a standard pipette and a single drop was manually gently deposited onto the oil surface. The mother drop was initially circular having a diameter of 3 mm then rapidly spread over the oil surface due to its high wettability. The evolution of the whole Marangoni bursting process was recorded with the digital video camera as well as with the IR thermal camera FLIR 96E (FLIR Systems, Inc., Wilsonville, OR, USA). The FLIR E96 thermal camera has been calibrated by the producer and the dedicated software FLIR Research Studio was used for data elaboration and analysis. The thermal camera is based on an uncooled microbolometer detector matrix (640 × 480 pixels, each 17 μm in size) detecting thermal radiation in the far infrared (FIR), i.e., at wavelengths between 7.5 and 14 μm with a temperature sensitivity of 30 mK at 303 K and an image frequency of 30 Hz. The accuracy of the temperature reading was given by the manufacturer as ±2 °C. This accuracy can

be improved by setting the thermal emissivity to the appropriate value for the studied material. Due to the multiphase nature of the studied material and its temporal changes due to alcohol evaporation, the value of thermal emissivity was set to 0.9. This was dictated by the fact that involved in our measurements thermal emissivities according to (https://www.thermoworks.com/emissivity-table/, accessed on 5 September 2023) are 0.95–1 for oil, 0.92–0.96 for water, 0.92–0.98 for alcohol and 0.85–0.95 for glass. The experiments were conducted at room temperature ~295 K and at relative humidity of 50–60%.

## 3. Results

### 3.1. Classic Marangoni Bursting Experiment

The exemplary Marangoni bursting phenomenon for $\phi_0$ = 0.45, IPA/water with brilliant blue dye was recorded as a video movie and a few frames from it marked with a time *t* (counted from the moment of contact of a binary mixture drop with oil phase) are shown in Figure 1. As seen in Figure 1, the mother drop of a volatile isopropanol and water solution with brilliant blue dye deposited at *t* = 0 s spreads spontaneously over the rapeseed oil surface within a few seconds. The high wettability of the initial droplet composition is the necessary condition to observe the unusual fingering instability appearing at the expanding and next receding mother droplet edge. This instability leads to the spontaneous segmentation process of the solution into tens or hundreds of smaller (millimeter or sub-millimeter in size) daughter droplets that detach and escape from the mother droplet's leading edge. Then, motile droplets move outside, and after approximately 13 s (for this particular composition), the process naturally slows down and droplet movement terminates. The conditions for the occurrence of this phenomenon can be summarized as follows: nonhomogeneous evaporation in a binary mixture, strong Marangoni stress, and a freely moving contact line on perfectly smooth surface [43–46].

The dynamics of Marangoni bursting is controlled by the continuous change in the surface tension of the alcohol/water mixture due to the evaporation of a more volatile component of the binary solution IPA/water. Isopropanol evaporates much faster than water—the IPA vapor pressure at 293 K is approximately 4.4 kPa, while that for water, at the same temperature, is only 2.34 kPa. IPA evaporation increases the surface tension of minute droplets, allowing their detachment at the ends of fingers, appearing at the mother drop edge and making them rounder, well separated, but also progressively smaller in size and weight during their movement toward the periphery area. Interestingly, after reaching the maximum distance *R* (outer ring *R* marked with red arrow in Figure 1) from the center, droplets do not rest but spontaneously return at much slower speed than during the expanding phase (see Figure 2). In this period, daughter droplets are slowly drifting over the oil surface, coalescing and tending to form a thin rim analogous to "coffee ring" effect observed for drying sessile droplet on a solid substrate [45–47]. The residual brilliant blue amorphous remnants of non-volatile dye resting on the oil surface can be observed after both alcohol and water complete evaporation, i.e., at a time longer than ~600 s. After this time, no further movement is observed at the oil pool surface. In summary, the three stages of the phenomenon can be distinguished: (i) fast mother drop spreading due to wetting of the oil surface, (ii) fingering instability followed by emulsification of binary solution and (iii) slow shrinking evolution of daughter droplets followed by the formation of the rim, composed of the remnants of dissolved in binary solution substance, on the oil surface.

Based on the work of Keiser et al. [30], Marangoni bursting is closely linked with the spreading coefficient *S*, defined as $S = \gamma_{oil-air} - \gamma_{mixture-air} - \gamma_{mixture-oil}$, where $\gamma$s are respective interfacial tensions. Parameter *S* must be positive to guarantee mother droplet spreading. This coefficient determines the energy per unit area of spreading and is counterbalanced by the viscous forces in the liquids. When the alcohol evaporation concentration of the binary mixture decreases below the critical fraction, and $\phi_c \approx 0.35$, the spreading parameter reaches zero (*S* = 0) and Marangoni bursting stops. Based on the

definition of *S*, it is obvious that even the subtle changes in the involved interfacial tensions $\gamma$s may influence the condition of generation or annihilation of Marangoni bursting.

The briefly described here phenomenon is qualitatively understood; however, forces involved in self-propulsion and the final evolution of the system are difficult describe quantitatively due to the complex coupling of solutal and thermal Marangoni stresses and hydrodynamical effects. Another difficulty comes from the mother and daughter droplet mass reduction due to the non-constant evaporation rate of alcohol and water. In this process, dynamic Marangoni mixing also occurs both close to the mother drop edge (at fingering instability region) as well as in daughter droplets moving over the oil surface. The role of dye and its concentration added for visualization purposes also needs further investigation. All these facts underline the complexity of the studied system, making the analytical description and the simulation of the phenomenon extremely difficult. Therefore, we limited our work to discussing Marangoni bursting in its final stage of slow movement, where unusual shrinking of the daughter droplet area over the oil surface was observed.

*3.2. Thermal Imaging of Marangoni Bursting in Dye-Free IPA/Water Binary Solution over Rapeseed Oil*

We started our investigations by repeating the experiment of Keiser et al. [30] for the IPA/water content ($\phi_0 = 0.45$) but without any dye (cf. Figure 2). Without the dye, the direct observation using a visible light color camera is difficult due to poor contrast. However, observation of Marangoni bursting by a thermal camera capable of monitoring surface temperature distribution is quite effective and carries information about the dynamics of temperature gradients arising during different stages of the process: spreading, wetting, emulsification, and finally water evaporation. This reference experiment differs from those performed with methyl blue dye added to the binary mixture prior to the Marangoni bursting observation.

In the sequence of photographs taken by a thermal camera, shown in Figure 2, we can observe a few characteristic events. When the drop of the IPA/water binary mixture ($\phi_0 = 0.45$) gently touches the oil surface, it starts to fast spread radially outwards over the surface (at 0.23 s) due to the strong wetting forces (small contact angle of the binary mixture with the oil surface). In this experiment, the initial temperature of the oil surface was approximately 23.5 °C. During binary mixture spreading, the initially small contact angle increases due to rapid evaporation of alcohol predominantly at the periphery of the droplet, which is marked by the blue color in Figure 2, signifying temperature decrease to ~21 °C (refer to the color temperature scale in Figure 2). Then, at some critical concentration difference, the spontaneous fingering instability appears at the edge of the initial/mother drop. Fingering instability starting at $t \approx 8.3$ s has led to the release of small daughter droplets. This process is hardly visible by the thermal camera in Figure 2 due to the fact that the instability wavelength $\lambda$ (the average distance between two neighboring fingers at the droplet edge circumference) is much smaller than that shown in Figure 1 and comparable to the spatial resolution of the thermal camera with the wide view germanium lens. With time, more and more daughter droplets are released and move in a radial fashion until their propelling force vanishes. The receding of the mother drop is observed until the whole mother drop is divided into daughter ones that occurred at time $t \approx 50$–60 s. After this outstanding phenomenon seizes, the daughter drops remaining on the oil surface evaporate, approaching each other, coalescing and drifting, forming a ring-like shape. At longer times, daughter droplets are mainly composed of water. Then, they migrate, forming an outer ring of radius R (at $t \sim 90$ s). This ring shrinks with a far smaller velocity than that observed in the initial expansion period. In the final stage (100–620 s), no alcohol is left in the droplets, and the system evolution is driven by water evaporation only, which is signified by the reddish–blue colors seen on the pool surface.

It has been experimentally confirmed that within 20–30 min, the ring disappears completely and under thermal camera view there are no more visible gradients of temperature. Based on the reference experimental findings shown in Figure 2, we plot the

dependence of the peripheric ring radius $R$ as a function of time and show it in Figure 3. Spreading of droplets over clean flat surfaces often obeys a power law growth of radius in time [41]: $R(t) \propto t^n$ with exponent $n = 0.75$. We observed generally similar behavior (Figure 3); however, the spreading exponent coefficient $n$ was estimated to be $n \approx 0.256$, i.e., $R(t) \propto t^{1/4}$. Interestingly, the process of shrinking of outer radius $R$ seems to obey the power law decay as well, and the shrinking exponent coefficient $n' \approx -0.356$ was estimated for the studied system (see the inset to Figure 3). We think that the fast alcohol evaporation causes this slowdown of peripheric ring expansion rate during Marangoni bursting over oil. This process induces, at the peripheric edge, thermal gradients resulting in immediate launching of counter flow of oil due to thermocapillary Marangoni stress that adds to pure viscous stress. Similar dependence $R(t) \propto t^n$ has been measured for the IPA/water binary mixture with $\phi_0 = 0.50$ (see Figure S5 of ESI) but the power low dependence $R(t) \propto t^n$ is different, we observed exponent $n = +0.3$ during the expansion period and exponent $n' = -0.3$ during the contraction phase.
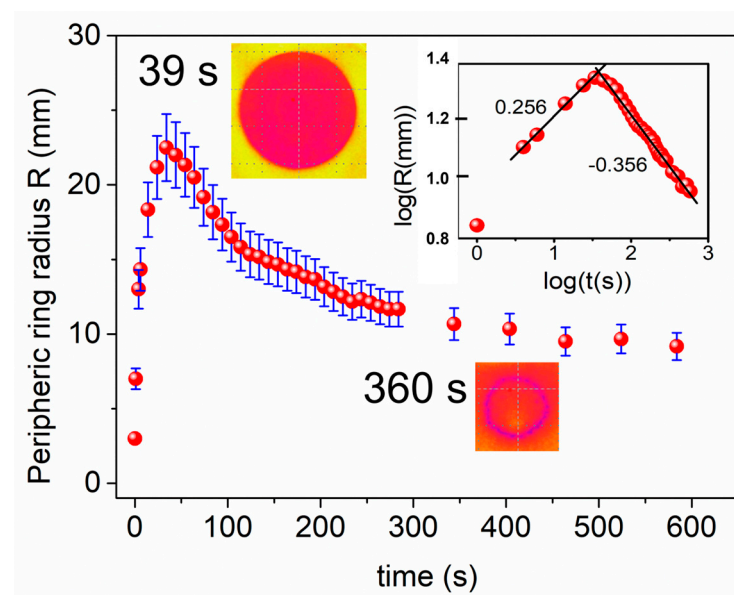


**Figure 3.** Dependence of outer ring radius R magnitude on time during the Marangoni bursting process, extracted from the snapshots taken from the respective movie. The IPA/water binary mixture was characterized by ($\phi_0 = 0.45$) and was deposited over pure rapeseed oil. The error bars come from the uncertainty of the evaluation of the diameter of the colder circular area on the oil surface. Inset shows the same plot but in a log–log scale (log(R) versus log(t)) with calculated exponent coefficients.

From the $R(t)$ dependence presented in Figure 3, we calculated the velocities $v(t) = \frac{\partial R}{\partial t}$ of the outer ring radius changes both in expansion and shrinkage periods and show them in Figure 4. The dynamics of the process is highly nonlinear, with maximum velocity reaching 7 mm·s$^{-1}$ at the beginning of spreading period and 0.1 to 0.003 mm·s$^{-1}$ in the receding of daughter droplets area and the final stage of ring shrinking, respectively. The detailed values of velocity depend on the initial mass fraction $\phi_0$ of the binary mixture and the oil properties. We postulate that the origin of the effect of slow movement and shrinking of daughter droplet area over the oil surface with time can be related to the thermocapillary Marangoni effect taking place on the oil surface but also in its volume due to momentum transfer. This supposition is validated by the observation of temperature gradients over the oil surface picked up by thermal camera until time ~600 s. Diddens et al. [46] in their work also observed that after the complete evaporation of alcohol from a binary mixture, strong Marangoni flows are still present. The phenomenon of the inward mass migration in a drying water droplet on a solid surface has been observed and described by Weon and Je [47], where the Marangoni effect reversed the coffee-ring effect.
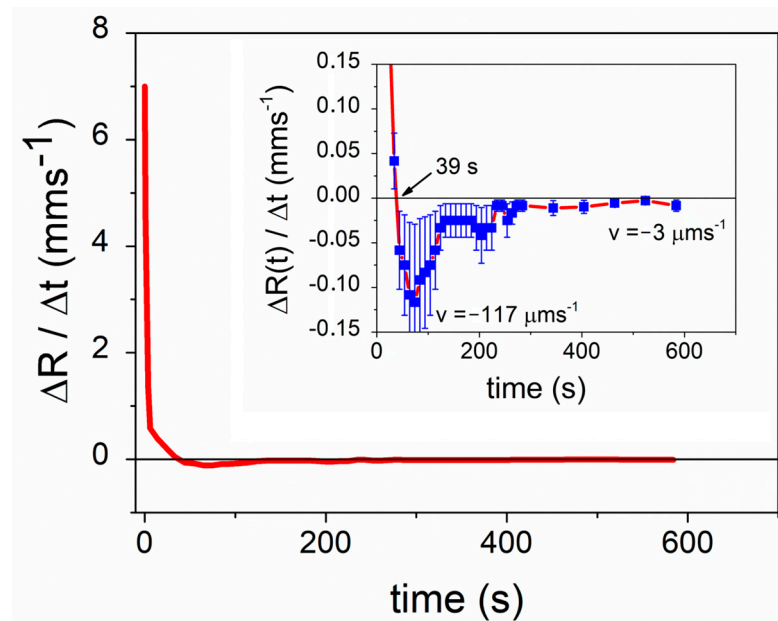
**Figure 4.** The velocity of outer ring $R$ expansion and shrinking $v(t) = \frac{\partial R}{\partial t}$ in the process of Marangoni bursting for IPA/water binary solution ($\phi_0 = 0.45$) deposited on rapeseed oil as calculated from the plot shown in Figure 3. Inset shows the details of the outer ring radius evolution in shrinkage period with the maximum speed of $v = -117\ \mu m \cdot s^{-1}$ and approximately $v = -3\ \mu m \cdot s^{-1}$ at time 500–600 s. The red line is a guide for an eye only and blue squares denote the exactly calculated velocities.

### 3.3. Thermal Imaging Study of Marangoni Bursting in IPA/Water Binary Solution Containing Methyl Blue Dye over Rapeseed Oil

Before discussing the results of Marangoni bursting in IPA/water binary solution studied with thermal camera, we present in Figure 5 the schematic view of the phenomenon, similar to that presented in [30], but underlining the role of the thermocapillary Marangoni effects both in binary solution as well as in the oil pool.

In Figure 5a, where the side view of the oil pool is schematically shown, the $R(t)$ (outer ring) describes the radius of the spreading thin layer of a binary mixture alternatively carrying daughter droplets generated in the fingering instability process. A smaller radius $r(t)$ denotes the edge extension of the mother drop from its center. The $j_v$ symbol describes the evaporation rate of alcohol and water, $\Delta T(x,y) = T_{surface}(x,y) - T_{ambient}(x,y)$ is the local temperature difference field over the oil surface, $\Delta \gamma(c)$ describes the local difference in binary solution concentration on the oil surface causing wetting spreading. $Ma_T$ denotes thermocapillary Marangoni flows in the oil phase (see the red arrows in Figure 5a, $\Delta F(t)$ describes the net force resulting from all the forces acting at the surface, $h_m$ is the thickness of the layer at the instability edge of the mother drop, and finally, $H$ is the thickness of the oil layer in the bath. The thickness of the oil layer cannot be too small; otherwise, Marangoni flows in the oil can be hampered. The red and blue horizontal arrows (Figure 5a) describe the counter-propagating near-surface streams of fluid mass in the oil phase. In Figure 5b, the simplified scheme of Marangoni bursting is shown as seen from the top; the white arrows inside the main droplet indicate the thermocapillary Marangoni flow in the binary mixture that causes the elongation of fingers outside the mother drop edge and promotes the droplet pinch-off outward the edge. It is clear from observations that instability wavelength $\lambda$ depends on time $\lambda(t)$ due to temporal dependence of alcohol/water concentration caused by faster evaporation of alcohol close to the droplet edges where the layer of solution is very thin ($h_m$). In Figure 5b, vectors of the speed of wetting $v_w(t)$ for expanding droplet edge and the velocity of retraction of the mother droplet edge $v_r(t)$ are also marked. Noticing the quite uniform temperature in between daughter droplets, we conclude that droplets are moving by sliding on a thin layer of the wetting binary mixture, at least in the initial phase of the phenomenon. By the nature of the recording infrared radiation, we can measure the

temperature of the investigated objects with an accuracy of only $\pm 2$ K. However, we were able to distinguish local dynamic changes in temperature with the precision of $\pm 0.1$ K at a rate of 30 frames per second. Detailed observations have shown that the wetting-driven flows are accompanied by thermocapillary effects acting at all stages of the development of macroscopic flower-shaped patterns. In Figure 6, we present the Marangoni bursting phenomenon seen by the thermal camera for the system with a binary mixture close to the critical IPA/water concentration $\phi_0 \approx \phi_c = 0.35$ that should result in the highest value of fingering instability wavelength $\lambda$.
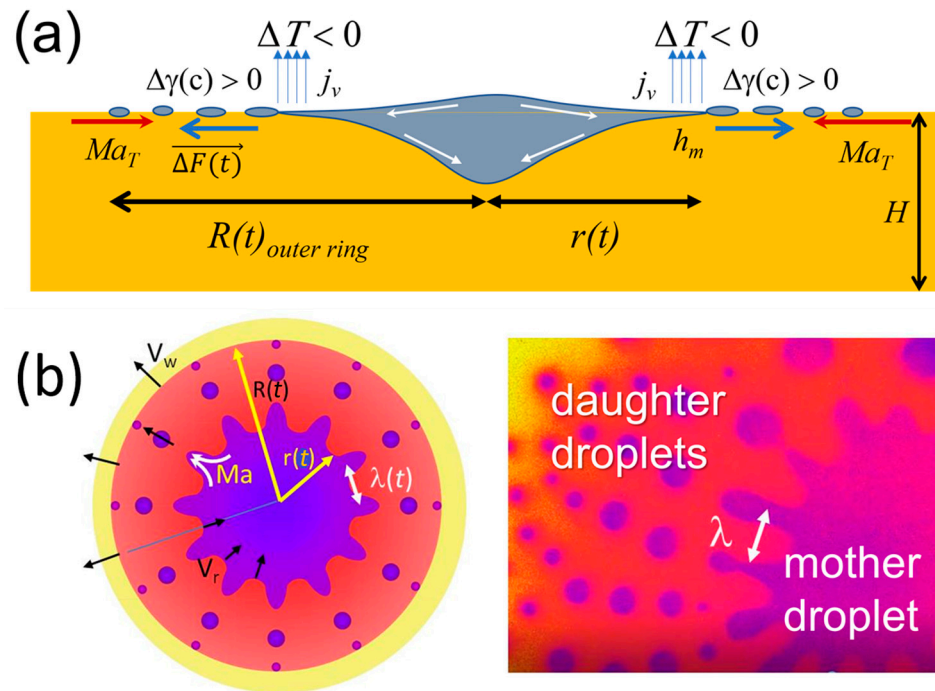


**Figure 5.** (**a**) Schematic view of the geometry of the Marangoni bursting experiment together with the main involved processes of wetting, evaporation, Marangoni thermocapillary effect and fingering instability resulting in droplets releasing. (**b**) Scheme of the top view of the same phenomenon where white arrows mark the Marangoni flows that pump binary solution liquid into fingers (ligaments). On the right side of the thermal image of the bursting phenomenon, the areas of mother and daughter droplets are added artificially to show the difference in surface temperature map $\Delta T(x,y) = T_{\text{surface}}(x,y) - T_{\text{ambient}}(x,y)$, where yellow color denotes higher temperature, red intermediate and blue the lowest one.

The goal was to gain insight into the temperature distribution in a separate ligament and separate daughter droplet with satisfactory thermal and spatial resolution. The sequence of events presented in Figure 6 shows that fingers are starting to be visible already at time $t = 1.287$ s with 26 fingers at the circumference while at time $t = 4.686$ s only 10 fingers can be identified. The area of deep-red color is assigned to the position of the wetting layer. The detachment of daughter droplets is not observed until time 2.28 s, and after this, the receding process of mother drop commences. Despite that, the large circular area with a clearly marked border has a lower temperature than the oil phase, suggesting a continuing evaporation process in this area. When the daughter droplet movement begins to be very slow, the droplets are seen as the separate centers of lower temperature circles floating over the uniform, a little warmer, thin evaporating layer of remnants of the initial solution (Figure 6 photos taken at 9.9 s and ~16 s). The nonuniform temperature distribution is seen in the mother drop as well as in larger daughter ones.
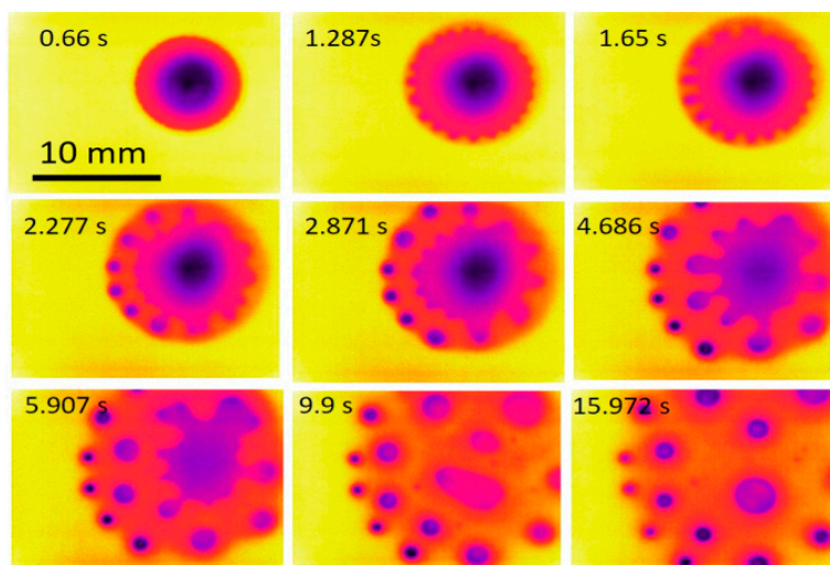
**Figure 6.** A sequence of thermal images captured from a movie during Marangoni bursting for IPA/water ($\phi_0 = 0.35$) on rapeseed oil within the time range of 0.66–16 s. The nonuniform temperature of each daughter drop ought to be noted. The scale bar is given in the first photograph. The deep blue color denotes the lowest surface temperature and the yellow the highest one, respectively. For the closer estimation of the temperature color meaning see the thermal analysis in Figure 7.
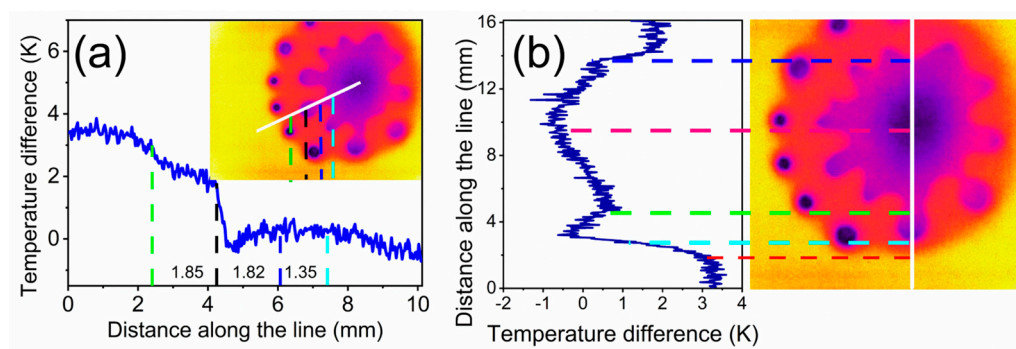


**Figure 7.** The detailed thermal analysis of IPA/water (initial $\phi_0 = 0.35$) droplets on rapeseed oil during the Marangoni bursting phenomenon. (**a**) The temperature cross-section (along the white line) through the whole droplet at t = 4.620 s is plotted on the left. (**b**) The temperature cross-section (along the white line) at the daughter droplet pinch-off moment at t = 4.686 s. The colored lines correspond to the temperature data points read from the thermal image at points of their crossing with the white line. The numbers inserted between the colored lines denote the real distance in millimeters between the temperature measurement points.

A closer analysis of the droplet pinch-off process as seen by the thermal camera is presented in Figure 7, where temperature changes are plotted against the distance along the chosen cut lines. The droplets forming at the finger ends have nonuniform temperature distribution across them, i.e., with the coldest area at their periphery (see Figure 7). The maximum magnitude of the temperature difference between the oil phase (at the bottom of Figure 7a) and the cold area at the finger periphery amounts to $\Delta T = 3.7$ K, while the maximum temperature difference between the oil phase and the mother drop center amounts to $\Delta T_{max} = 4.2$ K. The largest temperature gradient, $\nabla T \approx 3.5$ K·mm$^{-1}$, was observed at the daughter droplet edge just before the moment of its release (see also ESI Figure S1). Evidently, this proves that 2D thermocapillary Marangoni flows in the binary mixture are directed from the center toward mother droplet periphery. Similar temperature

gradients were reported by Hasegawa and Manzaki [43] and were postulated to drive the Marangoni stress.

Another cross-section (see white line in Figure 7b shows a similar sharp temperature decrease at the finger end, with the precisely determined temperature change in $\Delta T = -2.4$ K resulting in a temperature gradient $\nabla T \approx 6$ K·mm$^{-1}$. Thermal imaging shows that thermocapillary effects are superimposed on the wetting-driven flows. The wetting phenomenon of binary solution over the oil phase induces a process similar to Plateau–Rayleigh instability [48] known for the stream of falling water; however, gravity forces playing a role in Plateau–Rayleigh instability are replaced here by the forces tangential to the surface.

Then, at periodic locations at the mother droplet circumference, fluctuations in radial spreading led to the growth of fingers (shoots) of alcohol/water solution. The fingers are pushed outward and amplified by the Marangoni thermocapillary flows, as shown in Figure 5b by white arrows with Ma label. The shoots are being elongated and then, by minimizing their surface energy due to Laplace pressure [48], they spontaneously detach from the mother droplet, moving away, propelled by tangential wetting forces [49,50]. Ejection of subsequent droplets depletes the mother droplet volume, resulting in its inward retraction accompanied by further daughter droplet release. They, however, are moving at a much lower speed than during the initial expansion process. The temperature distribution along the chain of released daughter droplets is shown in ESI Figure S2; the droplets are colder than the surrounding surface temperature by ~1.3 K on average.

We observed the Marangoni bursting phenomenon with a thermal camera systematically for the different initial compositions of the binary mixture: $\phi_0 = 0.35$, 0.40, 0.45, 0.50, 0.55, 0.60 and 0.70 IPA/H$_2$O with methyl blue dye. Examples of these observations are attached in ESI as Video S1 ($\phi_0 = 0.40$), Video S2 ($\phi_0 = 0.45$), Video S3 ($\phi_0 = 0.50$), Video S4 ($\phi_0 = 0.60$) and Video S5 ($\phi_0 = 0.70$). For details of Marangoni kinetics in the expansion process for $\phi_0 = 0.70$, refer to Figure S3 and in the shrinking phase to Figure S4 of ESI. With the increase in the initial content of alcohol in the binary mixture, the continuous decrease in fingering instability wavelength $\lambda$ was observed (from mm to µm range) according to the earlier reported findings [31,44]. The initial concentration of alcohol in the binary mixture influences the wetting speed and therefore the process is faster for higher alcohol content. The decrease in the outer ring $R(t)$ as a function of time occurs for any of the studied systems. Interestingly, we have noticed that the shrinking of external ring $R(t)$ is accompanied by the removal of daughter droplets from the central part that was built after the complete vanishing of the mother drop. The process of drifting of daughter droplets pushed both from the outside as well as from the inside has attracted our attention and needs understanding. This process naturally ends with the formation of a thin ring. The described phenomenon is shown well in ESI Video S2 and is also shown in Figure 8 in the form of a sequence of photographs. In Figure 8, the process of the formation of a warmer region in the center of the initial deposition of the binary mixture drop is already seen at $t = 8.62$ s (see the appearance of a reddish area). Later on, the daughter droplets move radially out of the center ($t = 43.03$ s), forming finally a ring-like area of lower temperature.

The decrease in the outer ring radius and increase in the inner ring one finally leads to the formation of the thin cold ring, which stays at the same position until complete evaporation of water. The temperature difference between an oil surface with flowing daughter droplets and the area free of them results in the temperature gradient that drives the thermocapillary Marangoni effect in the oil phase. In the next subsection, we will model the flows in oil that forms the cold rings over the oil surface, as evidenced in Figure 8.
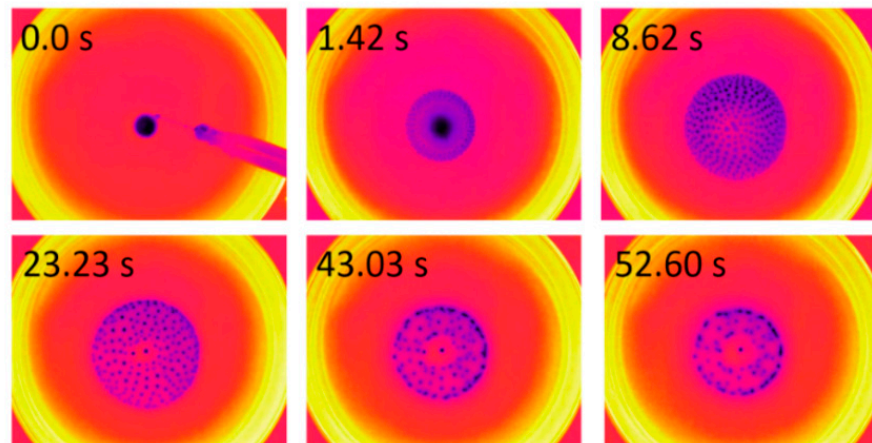
**Figure 8.** A sequence of photographs taken by thermal camera FLIR E96 during Marangoni bursting for the IPA/water mixture with $\phi_0 = 0.45$ on rapeseed oil. Blue color denotes the lowest and yellow the highest temperatures, respectively. Note the formation of outer and inner rims starting from $t = 23$ s.

### 3.4. Computer Fluid Dynamics Simulations of the Role of the Thermocapillary Marangoni Effect in Oil on Shrinking of the Outer Ring

The thermocapillary effect that accompanies the Marangoni bursting process is too complicated to be modeled; therefore, we simplify it to model the thermocapillary Marangoni effect due to the presence of static circular shape regions of lower temperature at the oil surface. For that purpose, we use the COMSOL Multiphysics 5.6 platform for performing Computer Fluid Dynamics simulations. We limited our simplified model to three cases (Figure 9a) by the artificial deposition of the uniform surface temperature over the oil surface: (i) the full cold circle (observed at 8.6 s in Figure 8); (ii) the cold ring (observed at 43 s in Figure 8); and (iii) the cold rim (observed at 600 s, not shown in Figure 8).

Initially, we assumed that the three areas have the same temperature that is lower than room temperature (295.3 K) by $\Delta T = -5$ K and is stable at least during the period of a few seconds. This is supported by the result shown in ESI (Figure S1), where the measured difference in temperature reached as much as $|7.5|$ K. Under such simplifications we solved in 3D the Navier–Stokes equations in laminar approximation coupled with heat transport equations. In Figure 9b,c, we show the results of simulations of $u_x$ and $u_z$ fluid flow velocity components at a line positioned slightly below the surface of an oil along the $x$-axis. It is obvious that flows in oil parallel to the surface are directed toward colder areas where the surface tension is higher, but it is not as evident that there is also a flow directed upward, i.e., along the $z$-axis (see Figure 9c). The response to the temperature gradient appearing at the oil surface is very fast; after only 0.05 s, the lateral flow velocity at the surface reaches value $|u_x| = 25$ mm·s$^{-1}$ and the vertical component $|u_z| = 7$ mm·s$^{-1}$. This is caused by the large thermal Marangoni shear stress: $\partial\gamma/\partial r = (\partial\gamma/\partial T)(\partial T/\partial r)$ assumed in our simplified model. By viscous momentum transfer, these fluid movements are generated also in the bulk of an oil pool.

In Figure 10, we show simulations which allow us to understand the mechanism of the slow shrinking of daughter droplets area. It is represented by a wide, colder ring similar to that observed in Figure 8 at $t = 43$ s. The simulation experiment geometry with cut line positioned along the $x$-axis slightly below the oil surface, surface temperature and fluid velocity fields are shown as a function of time in the range (0 to 4 s). Results of simulations qualitatively explain that the Marangoni fluid flows due to temperature gradients at the oil surface are responsible for the shrinking of the cold ring area of daughter droplets. They are acting from outside as well as from inside the ring as shown in Figure 10c. Fluid velocities directed outward the ring center are slightly smaller (<2 mm·s$^{-1}$) than those acting toward the center. This explains the reason for slow ring shrinking arising from the competition of two counter-propagating fluid flows. Therefore, the movement of daughter

droplets is very slow as compared to the initial phase in which they are created. Note, that almost instantly appearing Marangoni flows in oil cause temperature changes due to convective heat transport in the oil volume (see Figure 10b, where the multiple lines show the temperature evolution from the initial one at t = 0 s designed by the blue line). In Figure 10d, we can see that the fluid velocity component along the $z$-axis $u_z$ causes the mixing of oil in the bulk. The warmer oil from near the dish's walls moves down, while the volume of oil inside the ring moves up. The mixing reduces temperature gradients and causes the slowdown of the whole movement. The temperature gradients of cold liquid at the surface (evenly distributed) influence the oil bulk movements that tend to reduce the temperature gradients and finally form a smooth cold ring. Simulations performed for a narrow cold ring adequate to the final stage of shrinking are shown in ESI (Figure S6).
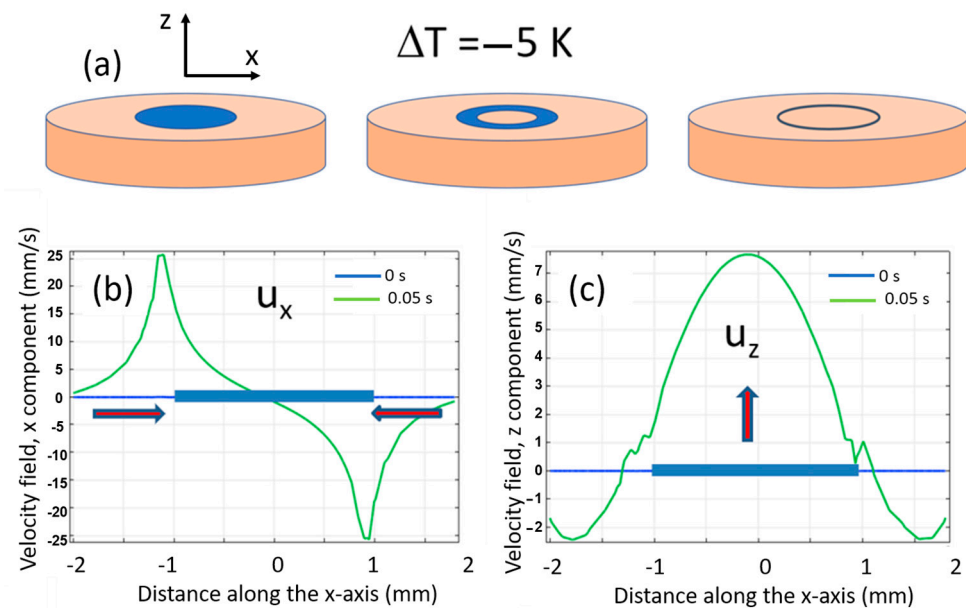


**Figure 9.** Simplified 3D simulations of thermocapillary Marangoni flow in the oil phase observed in the final stage of the Marangoni bursting phenomenon. (**a**) Simulated regions with lowered temperature by $\Delta T = -5$ K in the form of a circle, thick ring and narrow rim. (**b**) Flow velocity $u_x$ component of oil near the surface along the $x$-axis after deposition of a flat cold circular area at the oil pool surface. (**c**) Flow velocity $u_z$ component along the $x$-axis recorded near the surface. This flow appears in a short time (0.05 s) after the deposition of a flat, cold circular area at the oil pool surface. Here, the diameter of a pool is 4 mm, the oil layer height is 0.8 mm, and the center of the system is positioned at $x = 0$ mm and $y = 0$ mm.

The high-temperature difference $\Delta T = -5$ K used in the preliminary simulations presented in Figures 9 and 10 is not representative of the final stage of the process. Therefore, as proof of a principle, we performed full 3D simulations assuming a more realistic surface temperature decrease of only $\Delta T = -1.5$ K (Figure 11). We considered the case of daughter droplet ring-shaped area under the assumption that it is uniform and stable in time (at least within 10 s), again for the case observed in Figure 8 at $t = 43$ s. The geometry of simulation and heat exchange between the surface of oil and its bulk are shown in Figure 11a,b. In Figure 11c,d, instead of showing magnitudes of the velocities of fluid flows, we draw the vectors and streams, respectively. Representing velocity vectors are shown as red arrows centered in the midpoint. They show that the flow is directed from outside toward the center, but arrows perpendicular to the surface show that there is a flow of warmer oil from the bottom of a Petri dish to the surface. In Figure 11d, one can notice that closed loops of oil flows are present in the whole oil bulk. We may conclude that the two key fluid velocities (tangential and perpendicular to the surface) that are generated in the oil surface are responsible for gathering the daughter drops into the ring and then its shrinkage.
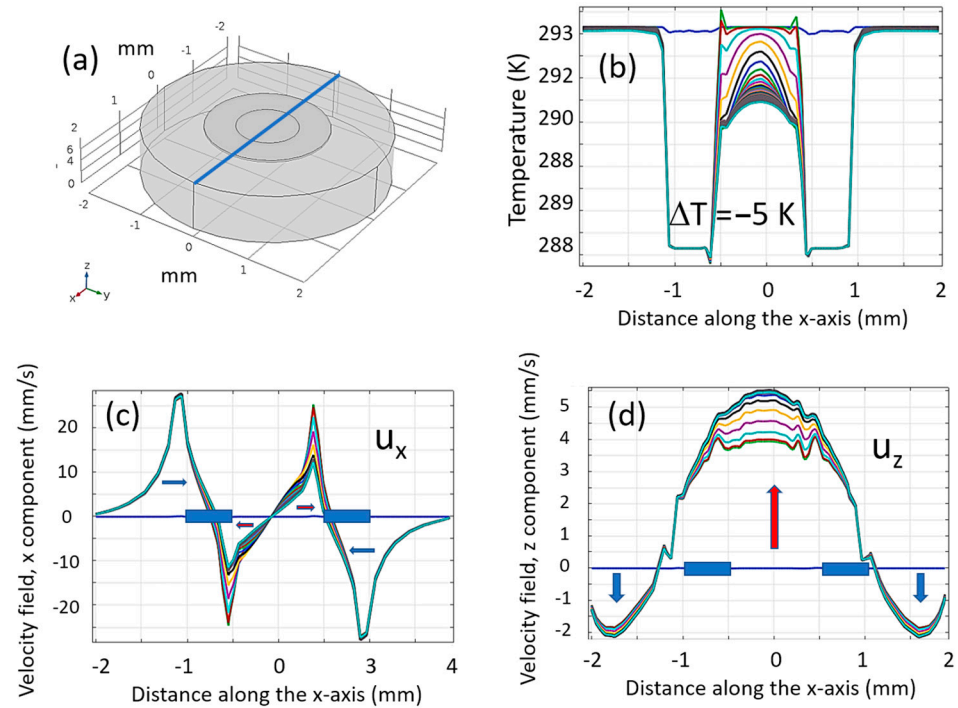
**Figure 10.** Simulations of the thermocapillary Marangoni effect in the late phase of Marangoni bursting phenomenon. (**a**) Oil pool with the cold ring deposited at the surface and the cut line along the *x*-axis. (**b**) Temperature evolution in the oil phase along the cut line for times from 0 to 4 s under the assumption of stable temperature $\Delta T = -5$ K imposed at $t = 0$ s. (**c**) Tangential velocity component $u_x$ of near-surface flows along the *x*-axis and its changes with time from $t = 0$ s to $t = 4$ s. (**d**) Velocity component $u_z$ measured along the *x*-axis as a function of time. Blue rectangular boxes represent the position of the cold ring over the oil surface. Color lines in (**b**) are drawn from time $t = 0$ s—blue line until $t = 4$ s with a period of 200 ms. Color lines in (**c**,**d**) are plotted each 400 ms in the time interval 0 to 4 s.

Simulations also show that the velocities of temperature gradient-driven Marangoni flows in rapeseed oil could be comparable to the wetting expansion velocities of the binary solution, i.e., approximately 32 mm·s$^{-1}$. These Marangoni flows have opposite directions to mother droplet movement during the bursting process and, therefore, must slow down the wetting propagation of the binary mixture over the liquid surface. We do not expect good matching between experiments and simulations due to the simplicity of the latter. However, we can estimate the influence of the thermocapillary Marangoni effect based on measured temperature gradients. Marangoni number describes the ratio between the advective transport rate of heat and its diffusive transport rate. By definition:

$$Ma = \gamma_T \cdot \frac{L \cdot \Delta T}{\mu \cdot \alpha_T} = \frac{\Delta\gamma \cdot L}{\mu \cdot \alpha_T} \qquad (1)$$

where $\gamma_T$ is the temperature coefficient of surface tension of substrate liquid, $\Delta T$ is the surface temperature difference along a distance L parallel to the surface at which the surface tension difference $\Delta\gamma$ has been built, $\mu$ is the dynamic viscosity, and $\alpha_T$ is the thermal diffusivity of the liquid. By equating the thermocapillary stress gradient $\frac{\Delta\gamma}{L}$ to the viscous stress $\frac{\mu u}{L}$, where $u$ is the speed of Marangoni flow, one obtains the speed of flow: $u \approx \frac{\Delta\gamma}{\mu}$. Assuming $\Delta T = 1.5$ K from the experiment and $\gamma_T = -0.0000758$ Nm$^{-1}$K$^{-1}$ for rapeseed oil the calculated surface tension difference amounts to $\Delta\gamma = 1.137 \times 10^{-4}$ Nm$^{-1}$. Then, $u \approx \frac{\Delta\gamma}{\mu} \approx 0.175$ ms$^{-1}$ where $\mu = 6.5 \times 10^{-4}$ Pa·s. Taking $L = 1$ mm, the theoretical value of Marangoni number amounts to $Ma = 1796 \approx 1800$. The observed flow velocities

of the outer ring edge movement are generally much smaller. However, in the case of Marangoni bursting they always result from the two competing counter propagating flows.
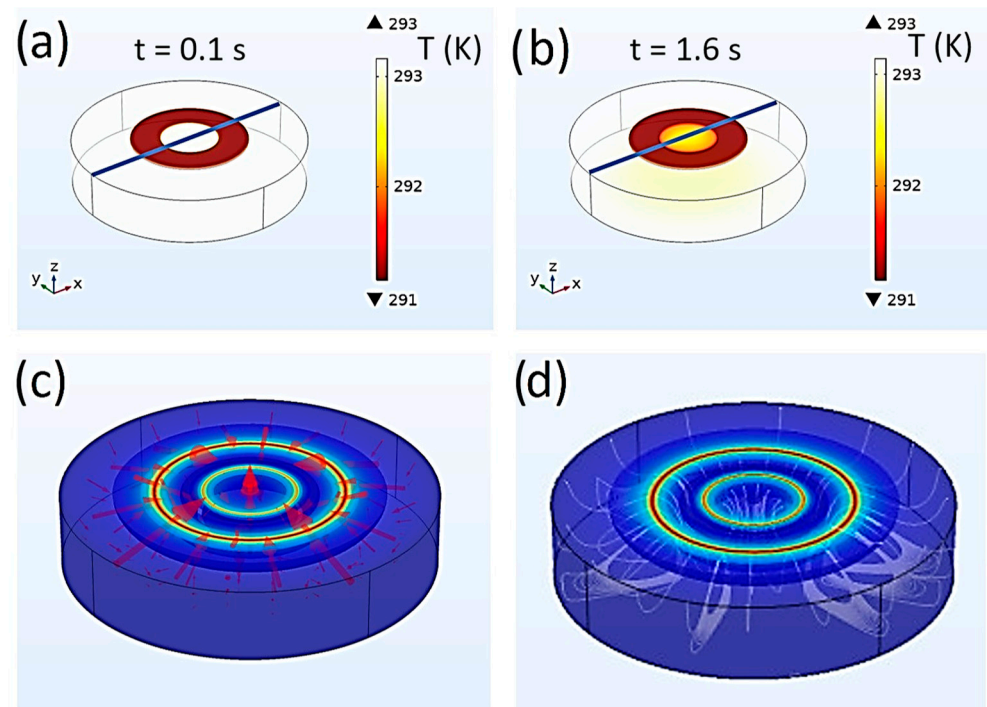


**Figure 11.** Exemplary 3D views of the geometry of the simulated oil pool system and a cross-section line position for which the local fluid flow velocities and temperature can be calculated. (**a**) Temperature distribution due to a cold ring at *t* = 0.1 s counted from deposition of lower by ΔT = −1.5 K. (**b**) Temperature distribution due to a cold ring after *t* = 1.6 s. (**c**) Thermocapillary Marangoni fluid flow velocities in an oil bath at *t* = 1.6 s represented by proportional vectors (red arrows). (**d**) Closed-loop stream lines in the oil bulk are forming, at *t* = 1.6 s, Bénard–Marangoni-like cells. The colors represent the surface velocity field with blue denoting the lowest velocity and red the highest one.

Thus, we can conclude that the thermocapillary Marangoni effect is important in Marangoni bursting from the very first moment of droplet deposition on the oil substrate until the formation of non-movable ring at the end of the phenomenon. The Marangoni flows that are dependent on temperature gradients play an important role in fingering process at the droplet edge. When the oil layer thickness becomes too thin, the loops of liquid flow have difficulty to build up because of hampering the fluid speed at the bottom of the Petri dish (note that in the simulations we used no-slip conditions).

## 4. Discussion

The beauty and regularity of the droplet-releasing phenomenon as observed in Marangoni bursting provoked many interesting studies of the different aspects of the phenomenon. Our work was not aimed to develop any theory of this complex behavior but to understand the evolution of the Marangoni bursting phenomenon after the initially dominating solutal Marangoni spreading [50] disappears. However, the remaining daughter droplets still drift over the surface in a predictable fashion, i.e., shrinking and forming a double-rim structure and ending with a single rim. An excellent study of the importance of thermal Marangoni-driven spreading and receding of a volatile droplet on an oil pool has been recently published by Jaberi et al. [51]. The conclusion of the thorough study using infrared thermography and theory is that the behavior is the result of competition between

solutal and thermal Marangoni stresses acting opposite to each other. This conclusion is in accordance with our measurements, too.

The table with collected liquid physicochemical parameters of IPA and oil used in experiments is given in ESI (Tables S1 and S2). In any Marangoni bursting phenomenon observed by infrared thermography, the value of surface tension changed with time, then also $\gamma_T$ of the binary mixture. Note that at 293.15 K, the surface tension of isopropanol $\gamma_{IPA} = 23.0$ mN·m$^{-1}$ and the thermal coefficient of surface tension $\gamma_{T,IPA} = -0.078$ mN·m$^{-1}$ K$^{-1}$, whereas for water $\gamma_{H2O} = 72.80$ mN·m$^{-1}$ and thermal coefficient of surface tension $\gamma_{T, H2O} = -0.151$ mN m$^{-1}$ K$^{-1}$. These values are quite different, and they have a dynamic impact on the shape and thickness of the mother droplet edge during the process and evaporation rate. Thus, the wavelength of instability length $\lambda$ is indirectly dependent on the surface tension of the mother droplet and regulates the size and number of detaching daughter droplets. We performed measurements of the dependence of the surface tension $\gamma(\phi_0)$ on the initial values of volumetric IPA contents in water. The experimental curve is shown in ESI (Figure S3), and the numerical fitting procedure with a single exponential function gave an approximate formula:

$$\gamma(\phi_0) = 47.75 \cdot \exp\left(-\frac{\phi_0}{12.66}\right) + 24.61 \qquad (2)$$

in units of mN·m$^{-1}$. Although Marangoni bursting appears only in the range of $\phi_0 \sim 0.35$–0.85, the function may prove useful when discussing solutions outside this range.

The future study of the final stage of Marangoni bursting can be linked with a novel microcrystal growth method. The tiny droplets formed during Marangoni bursting at high alcohol content in the initial binary mixtures can carry the nanogram number of substances dissolved in alcohol or water prior to the experiment. After droplet evaporation, dissolved substances may crystallize into nanocrystals or form other nanoassemblies [52]. The fingering instability is not limited to liquid-phase substrate only; it is also observed on solid substrates [53], showing promise for application in nanocrystal growth techniques or polymeric periodic structure formation [54].

## 5. Conclusions

We described the simple system of alcohol/water/rapeseed oil in which the spontaneous formation of up to millions of droplets may take place within tens of seconds. The described process of Marangoni bursting requires the use of a well-chosen binary solution of alcohol and water as well as a liquid substrate free from any defects, e.g., such as an oil surface. The spatiotemporal changes in the surface tension caused by the concentration and temperature gradients result in spatially periodic spreading motions at the surface. We observed the behavior of this system from the perspective of temperature changes during the process. Wetting spreading of a binary mixture is definitely the driving force in the initial phase of the phenomenon; however, temperature gradients and the thermocapillary Marangoni effect in the binary mixture as well as in the oil phase influence both the formation of fingers and the formation of the long-term (up to 10 min) behavior of the system until its rest. Thermal imaging reveals the existence of temperature gradients of sufficient magnitude to induce Marangoni stress able to compete with that of concentration gradients.

We explained the second stage of the phenomenon that has not been mentioned in the literature before—the shrinking of daughter drops assembly drifting over the oil surface, and formation of the ring. We hope that our experimental study will shed new light on the dynamics of the system and explain, with the help of computational fluid dynamic simulations of the thermocapillary Marangoni effect in the volume of the oil pool, the evolution of the process at its final phase.

## References

1. James Thomson, A.M.C.E. On certain curious Motions observable at the Surfaces of Wine and other Alcoholic Liquors. *Lond. Edinb. Dublin Philos. Mag. J. Sci.* **1855**, *10*, 330–333. [CrossRef]
2. Marangoni, C. *Sull'espansione Delle Goccie d'un Liquido Galleggianti Sulla Superficie di Altro Liquido [On the Expansion of a Droplet of a Liquid Floating on the Surface of Another Liquid]*; Fratelli Fusi: Pavia, Italy, 1869.
3. Marangoni, C. The principle of the surface viscosity of liquids established by J. Plateau. *Il Nuovo C. Ser.* **1872**, *2*, 239.
4. Venerus, D.C.; Simavilla, D.N. Tears of wine: New insights on an old phenomenon. *Sci. Rep.* **2015**, *5*, 16162. [CrossRef] [PubMed]
5. Mills, K.C.; Keene, B.J.; Brooks, R.F.; Shirali, A. Marangoni effects in welding. *Philos. Trans. R. Soc. Lond. Ser. A Math. Phys. Eng. Sci.* **1998**, *356*, 911–925. [CrossRef]
6. Xiao, B.; Zhang, Y. Marangoni and Buoyancy Effects on Direct Metal Laser Sintering with a Moving Laser Beam. *Numer. Heat Transf. A Appl.* **2007**, *51*, 715–733. [CrossRef]
7. Aucott, L.; Dong, H.; Mirihanage, W.; Atwood, R.; Kidess, A.; Gao, S.; Wen, S.; Marsden, J.; Feng, S.; Tong, M.; et al. Revealing internal flow behaviour in arc welding and additive manufacturing of metals. *Nat. Commun.* **2018**, *9*, 5414. [CrossRef]
8. Marra, J.; Huethorst, J.A.M. Physical principles of Marangoni drying. *Langmuir* **1991**, *7*, 2748–2755. [CrossRef]
9. Li, C.; Zhao, D.; Wen, J.; Cheng, J.; Lu, X. Evolution of entrained water film thickness and dynamics of Marangoni flow in Marangoni drying. *RSC Adv.* **2018**, *8*, 4995–5004. [CrossRef]
10. Lee, S.B.; Lee, S.; Kim, D.G.; Kim, S.H.; Kang, B.; Cho, K. Solutal-Marangoni-Flow-Mediated Growth of Patterned Highly Crystalline Organic Semiconductor Thin Film Via Gap-Controlled Bar Coating. *Adv. Funct. Mater.* **2021**, *31*, 2100196. [CrossRef]
11. Stetten, A.Z.; Iasella, S.V.; Corcoran, T.E.; Garoff, S.; Przybycien, T.M.; Tilton, R.D. Surfactant-induced Marangoni transport of lipids and therapeutics within the lung. *Curr. Opin. Colloid Interface Sci.* **2018**, *36*, 58–69. [CrossRef]
12. Hsieh, M.-H.; Wei, H.-J.; Chen, K.-H.; Wang, H.-C.; Yu, C.-H.; Lu, T.-H.; Sung, H.-W. A fast and facile platform for fabricating phase-change materials-based drug carriers powered by chemical Marangoni effect. *Biomaterials* **2021**, *271*, 120748. [CrossRef]
13. Nerger, B.A.; Brun, P.-T.; Nelson, C.M. Marangoni flows drive the alignment of fibrillar cell-laden hydrogels. *Sci. Adv.* **2020**, *6*, eaaz7748. [CrossRef] [PubMed]
14. Takeuchi, H.; Motosuke, M.; Honami, S. Noncontact Bubble Manipulation in Microchannel by Using Photothermal Marangoni Effect. *Heat Transf. Eng.* **2012**, *33*, 234–244. [CrossRef]
15. Kitamura, I.; Oishi, K.; Hara, M.; Nagano, S.; Seki, T. Photoinitiated Marangoni flow morphing in a liquid crystalline polymer film directed by super-inkjet printing patterns. *Sci. Rep.* **2019**, *9*, 2556. [CrossRef] [PubMed]
16. Karbalaei, A.; Kumar, R.; Cho, H. Thermocapillarity in Microfluidics—A Review. *Micromachines* **2016**, *7*, 13. [CrossRef]
17. Lin, L.; Peng, X.; Mao, Z.; Li, W.; Yogeesh, M.N.; Rajeeva, B.B.; Perillo, E.P.; Dunn, A.K.; Akinwande, D.; Zheng, Y. Bubble-Pen Lithography. *Nano Lett.* **2016**, *16*, 701–708. [CrossRef]
18. Lv, C.; Varanakkottu, S.N.; Baier, T.; Hardt, S. Controlling the Trajectories of Nano/Micro Particles Using Light-Actuated Marangoni Flow. *Nano Lett.* **2018**, *18*, 6924–6930. [CrossRef]
19. Günther, A.; Jensen, K.F. Multiphase microfluidics: From flow characteristics to chemical and materials synthesis. *Lab Chip* **2006**, *6*, 1487–1503. [CrossRef]

20. Vernay, C.; Ramos, L.; Ligoure, C. Bursting of Dilute Emulsion-Based Liquid Sheets Driven by a Marangoni Effect. *Phys. Rev. Lett.* **2015**, *115*, 198302. [CrossRef]
21. Berg, S. Marangoni-driven spreading along liquid-liquid interfaces. *Phys. Fluids* **2009**, *21*, 032105. [CrossRef]
22. Yamamoto, D.; Nakajima, C.; Shioi, A.; Krafft, M.P.; Yoshikawa, K. The evolution of spatial ordering of oil drops fast spreading on a water surface. *Nat. Commun.* **2015**, *6*, 7189. [CrossRef]
23. Svitova, T.F.; Hill, R.M.; Radke, C.J. Spreading of aqueous trisiloxane surfactant solutions over liquid hydrophobic substrates. *Langmuir* **2001**, *17*, 335–348. [CrossRef]
24. Hamraoui, A.; Cachile, M.; Poulard, C.; Cazabat, A.M. Fingering phenomena during spreading of surfactant solutions. *Colloid Surf. A Physicochem. Eng. Asp.* **2004**, *250*, 215–221. [CrossRef]
25. Mollaei, S.; Darooneh, A.H. Spreading, fingering instability and shrinking of a hydrosoluble surfactant on water. *Exp. Therm. Fluid Sci.* **2017**, *86*, 98–101. [CrossRef]
26. Chowdhury, D.; Sarkar, S.P.; Kalita, D.; Sarma, T.K.; Paul, A.; Chattopadhyay, A. Spreading and recoil of a surfactant-containing water drop on glass-supported alcohol films. *Langmuir* **2004**, *20*, 1251–1257. [CrossRef] [PubMed]
27. Van Nierop, E.A.; Ajdari, A.; Stone, H.A. Reactive spreading and recoil of oil on water. *Phys. Fluids* **2006**, *18*, 038105. [CrossRef]
28. Eggers, J.; Villermaux, E. Physics of liquid jets. *Rep. Prog. Phys.* **2008**, *71*, 036601. [CrossRef]
29. Fanton, X.; Cazabat, A.M. Spreading and instabilities induced by a solutal Marangoni effect. *Langmuir* **1998**, *14*, 2554–2561. [CrossRef]
30. Keiser, L.; Bense, H.; Colinet, P.; Bico, J.; Reyssat, E. Marangoni Bursting: Evaporation-Induced Emulsification of Binary Mixtures on a Liquid Layer. *Phys. Rev. Lett.* **2017**, *118*, 074504. [CrossRef]
31. Video—Liquid Drop Bursts into Thousands of Pieces. (Link to Video Showing Marangoni Bursting Phenomenon). Available online: https://physics.aps.org/articles/v10/19 (accessed on 16 March 2023).
32. Wodlei, F.; Sebilleau, J.; Magnaudet, J.; Pimienta, V. Marangoni-driven flower-like patterning of an evaporating drop spreading on a liquid substrate. *Nat. Commun.* **2018**, *9*, 820. [CrossRef]
33. Pinto, R.L.; Le Roux, S.; Cantat, I.; Saint-Jalmes, A. Enhanced interfacial deformation in a Marangoni flow: A measure of the dynamical surface tension. *Phys. Rev. Fluids* **2018**, *3*, 024003. [CrossRef]
34. Durey, G.; Kwon, H.; Magdelaine, Q.; Casiulis, M.; Mazet, J.; Keiser, L.; Bense, H.; Colinet, P.; Bico, J.; Reyssat, E. Marangoni bursting: Evaporation-induced emulsification of a two-component droplet. *Phys. Rev. Fluids* **2018**, *3*, 100501. [CrossRef]
35. Motaghian, M.; Shirsavar, R.; Erfanifam, M.; Sabouhi, M.; van der Linden, E.; Stone, H.A.; Bonn, D.; Habibi, M. Rapid spreading of a droplet on a thin soap film. *Langmuir* **2019**, *35*, 14855. [CrossRef]
36. Kim, S.; Kim, J.; Kim, H.-Y. Dewetting of liquid film via vapour-mediated Marangoni effect. *J. Fluid Mech.* **2019**, *872*, 100–114. [CrossRef]
37. Mouat, A.P.; Wood, C.E.; Pye, J.E.; Burton, J.C. Tuning Contact Line Dynamics and Deposition Patterns in Volatile Liquid Mixtures. *Phys. Rev. Lett.* **2020**, *124*, 064502. [CrossRef]
38. Lohse, D.; Zhang, X. Physicochemical hydrodynamics of droplets out of equilibrium. *Nat. Rev. Phys.* **2020**, *2*, 426. [CrossRef]
39. Ma, X.; Zhong, M.; He, Y.; Liu, Z.; Li, Z. Fingering instability in Marangoni spreading on a deep layer of polymer solution. *Phys. Fluids* **2020**, *32*, 112112. [CrossRef]
40. Villermaux, E. Fragmentation versus cohesion. *J. Fluid Mech.* **2020**, *898*, P1. [CrossRef]
41. Williams, A.G.L.; Karapetsas, G.; Mamalis, D.; Sefiane, K.; Matar, O.K.; Valluri, P. Spreading and retraction dynamics of sessile evaporating droplets comprising volatile binary mixtures. *J. Fluid Mech.* **2020**, *907*, A22. [CrossRef]
42. Diddens, C.; Li, Y.; Lohse, D. Competing Marangoni and Rayleigh convection in evaporating binary droplets. *J. Fluid Mech.* **2021**, *914*, A23. [CrossRef]
43. Hasegawa, K.; Manzaki, Y. Marangoni fireworks: Atomization dynamics of binary droplets on an oil pool. *Phys. Fluids* **2021**, *33*, 034124. [CrossRef]
44. Seyfert, C.; Marin, A. Influencee of added dye on Marangoni-driven droplet instability. *Phys. Rev. Fluids* **2022**, *7*, 043602. [CrossRef]
45. Mampallil, D.; Eral, H.B. A review on suppression and utilization of the coffee-ring effect. *Adv. Colloid Interface Sci.* **2018**, *252*, 38–54. [CrossRef]
46. Diddens, C.; Kuerten, J.G.M.; Van der Geld, C.W.M.; Witten, T.A. Modeling the evaporation of sessile multi-component droplets. *J. Colloid Interface Sci.* **2017**, *487*, 426–436. [CrossRef]
47. Weon, B.M.; Je, J.H. Capillary force repels coffee-ring effect. *Phys. Rev.* **2010**, *82*, 015305. [CrossRef]
48. Gennes, P.-G.; Brochard-Wyart, F.; Quéré, D. *Capillary and Wetting Phenomena—Drops, Bubbles, Pearls, Waves*; Reisinger, A., Translator; Springer: New York, NY, USA, 2002.
49. Bonn, D.; Eggers, J.; Indekeu, J.; Meunier, J.; Rolley, E. Wetting and spreading. *Rev. Mod. Phys.* **2009**, *81*, 739–805. [CrossRef]
50. Fraaije, J.G.E.; Cazabat, A.M. Dynamics of spreading on a liquid substrate. *J. Colloid Interface Sci.* **1989**, *133*, 452–460. [CrossRef]
51. Jaberi, A.; Debenest, G. Plouraboué, Marangoni-driven spreading and receding of a volatile droplet on a liquid layer. *Phys. Rev. Fluids* **2023**, *8*, 073601. [CrossRef]
52. Cai, Y.; Newby, B.Z. Marangoni Flow-Induced Self-Assembly of Hexagonal and Stripelike Nanoparticle Patterns. *J. Am. Chem. Soc.* **2008**, *130*, 6076–6077. [CrossRef]

53.  Doumenc, F.; Guerrier, B. Self-patterning induced by a solutal Marangoni effect in a receding drying meniscus. *Europhys. Lett.* **2013**, *103*, 314–318. [CrossRef]
54.  Weh, L. Surface Structures in Thin Polymer Layers Caused by Coupling of Diffusion-Controlled Marangoni Instability and Local Horizontal Temperature Gradient. *Macromol. Mater. Eng.* **2005**, *290*, 976–986. [CrossRef]